2016-11-14

Rapid mantle-driven uplift along the Angolan margin in the late Quaternary

Walker, RT

http://hdl.handle.net/10026.1/6776

10.1038/ngeo2835
Nature Geoscience
Springer Science and Business Media LLC

Rapid mantle-driven uplift along the Angolan margin in the late Quaternary

R. T. Walker[1], M. Telfer[2], R. L. Kahle[3], M. W. Dee[4], B. Kahle[3], J.-L. Schwenninger[4] R. A. Sloan[3], A. B. Watts[1]

1) Department of Earth Sciences, Oxford University, South Parks Road, Oxford, OX1 3AN

2) School of Geography, Earth and Environmental Sciences, Plymouth University, Drake Circus, Plymouth, Devon, PL4 8AA

3) Department of Geological Sciences, University of Cape Town, Rondesbosch 7701, South Africa

4) Research Laboratories for Archaeology and the History of Art, Oxford University, South Parks Road, Oxford,

It is recognized that mantle flow can cause the Earth's surface to uplift and subside, but the rates and durations of these motions are, in general, poorly resolved due to the difficulties in making measurements of relatively small vertical movements (hundreds of metres) over sufficiently large distances (~1000 km). Here we examine the effect of mantle upwelling through a study of Quaternary uplift along the coast of Angola. Using both optically-stimulated luminescence on sediment grains, and radiocarbon dating of fossil shells, we date a 25 m coastal terrace at ~45 ka, when sea level was ~75 m lower than today, indicating a rapid uplift rate of 1.8-2.6 mm/yr that is an order of magnitude higher than previously obtained rates averaged over longer time periods. Automated extraction and correlation of coastal terrace remnants from digital topography uncovers a symmetrical uplift with diameter of >1000 km. The wavelength and relatively short timescale of the uplift suggest it is associated with a mantle process, possibly convective upwelling, and that the topography may be modulated by rapid short-lived pulses of mantle-

derived uplift. Our study shows that stable continental regions far from the effects of glacial rebound may experience rapid vertical displacements of several millimetres per year.

It is a long held view that sea-level changes along mature continental margins, far from tectonic activity and glacial loading, represent global (eustatic) variations (e.g.[1]). However, there is a growing realization that vertical motions at the Earth's surface may occur in the absence of lithospheric (plate tectonic) processes, and are instead driven by forces introduced by convection in the sub-lithospheric mantle (e.g. [2]). Many studies have focused on Africa, which has a long-wavelength topography composed of broad swells and basins, occurring both within the continental interior and at its margins (e.g. Fig. 1a-b) [3]. However, there is a range of interpretations of the origin of these topographic swells, from 'dynamic' causes of mantle upwelling, through flank uplift to adjoining subsiding basins, to the isostatic response to near surface density contrasts (e.g.[2-9]). The remaining challenge for understanding the origin of these events is the quantification of their rates, durations, and extents.

We focus on the coastline of Angola (Fig. 1c). Cenozoic uplift is recorded in the large-scale topography and drainage patterns, in offshore sedimentation and denudation, and in the emergence of Quaternary marine and coastal sediments[7; 8; 10; 11]. Much of central Angola is occupied by the Bié plateau, a dome-shaped range of ~1000 km diameter, rising to an elevation of >2500 m (Fig. 1c). Inverse modelling of river profiles on the plateau flanks yield two uplift 'pulses', with rates of up to 0.5 mm/yr, and with durations of ~1 Ma[8]. Pulses of tilting and denudation in the mid-Oligocene (30-35 Ma) and post-Pliocene are also observed in seismic reflection profiles across the Angolan continental shelf[7].

Pleistocene coastal uplift is demonstrated by Gilbert-type delta systems adjacent to the Kwanza and Benguela rivers (Fig. 1c). Coastal terraces representing late Quaternary uplift are observed adjacent to the Bié dome and the offshore regions that preserve evidence of Cenozoic denudation[7; 8; 10; 11]. The marine terraces extend smoothly for long distances[10] suggesting that active faulting, salt movements, and sediment loading are not the ultimate cause, and that deep, i.e. mantle, processes may instead be responsible. Existing age data for the terraces have been used to suggest relatively rapid uplift, accelerating from ~0.3 mm/yr at ~100 ka to 1.7 mm/yr over the last ~30 ka [10,11]. This is an order of magnitude higher than longer-term uplift rates from this region[7,8], or from most[12,13], though not all[14,15], studies of long wavelength topography elsewhere. The existing estimates of late Pleistocene uplift in Angola are based primarily on unreliable dating methods, demanding skepticism and careful documentation. Here, we examine the late Pleistocene rates and extent of uplift inferred from coastal terraces through a program of age dating and regional correlation.

Pleistocene terraces of the Angolan coast

The Angolan coastal terraces were first recognized and described by[16]. Near Benguela they are observed up to ~250 m, including several prominent intermediate levels[10; 11] (Fig. 1d and Supplementary Figure 1). The 120 m terrace contains Acheulian lithics and has a single U-series age of 200 ka[10]. A relatively indistinct ~50 m terrace has been interpreted as the penultimate interglacial[10]. The 25 m level has U-series dates ranging from 71 ka to 112 +/- 6 ka[10]. A terrace at ~10 m elevation has U-series ages of ~36 ka and radiocarbon ages of ~25 ka[10]. However, uplift rates derived from the ages are unlikely to be correct as U-series dating of mollusc shells is known to be unreliable (e.g.[17]).

The uplifted coastal terraces end northwards by the Congo estuary, do not extend south of central Namibia[18] (Fig. 1c), and peak near Benguela[10, 11]. The existing studies of the terrace sequences are unable to directly correlate the terrace fragments, which are separated by large longitudinal distances, justifying the approach of mapping and correlation from remote-sensing.

Our field study focused on the 25 m terrace, which is well exposed close to Benguela, and which has a relatively simple geomorphic expression. We sampled the terrace at three localities (A-C; Fig. 1d). The terrace is composed of an abrasion surface in soft early Tertiary mudstones that is overlain by lagoonal, beach and near-shore sediments. We interpret the abrasion surface and sedimentary cover to result from a single sea level excursion with several thousand years duration. The sediments do not contain corals that would generate reliable U-series ages, but are rich in quartz sand grains that can be dated with optically-stimulated luminescence (OSL). Several recent studies have shown the utility of OSL dating of coastal sediments (e.g.[19;20;21]). We collected eight OSL samples from the 25 m terrace, using appropriate protocols to minimize any possible partial bleaching effects. We also collected bivalve shells from the terrace deposits for radiocarbon dating. The sampling methods and analytical procedures are described in Methods. Additional information relating to the field sites and dating results are given as supplementary information (Supplementary Figs. 2-3; Supplementary Tables 1-2).

25 m terrace site descriptions and age constraints

The first of our sampling sites (Site A on Fig. 1d, corresponding to location AN-54 in[10]) is located in a river cutting ~5 km southwest of Benguela. A wide erosional platform cut into early Tertiary mudstone is overlain by ~2 m thickness of Quaternary sediments (Supplementary Figs. 2-3). The lower part of the sequence is composed of dark and finely-laminated sand/silt. The microfaunal assemblage at Site A contains species indicative of brackish to marine environments[10]. Two U-series ages of 112 +/- 6 ka and 103 +/- 5 ka are reported from bivalve shells[10]. We collected four OSL samples. We also collected a number of shells from the deposit, of which two (*Arca sp.* and *Ostreida sp.*) were selected for radiocarbon dating. We took another two OSL samples from Site B, located just north of Benguela at 12º33'03.2''S 13º26'22.7''E (Supplementary Figs. 2-3). The presence of heavily-ribbed bivalves at Site B indicates high-energy near-shore environments. A single OSL sample (BNG10-12) was collected from Site C, situated behind the Benguela football stadium, at 12º32'39.4''S 13º27'50.6''E (Supplementary Figs. 2-3). The fauna at Site C was predominantly *Arca sp.*. Gypsiferous horizons indicate a similar lagoonal environment to that interpreted for Site A[10].

The eight OSL ages from the 25 m terrace range in age from 57.8 +/- 11.2 ka to 36.8 +/- 3.4 ka (Fig. 2, also see Methods, Supplementary Table 1, Supplementary Figure 3). Our results confirm that the terrace is much younger than previously thought, and showing that uplift rates based on the U-series ages are not reliable. For the radiocarbon dating (see Methods and Supplementary Table 2), oceanic upwelling adjacent to our field site will lead to reservoir effects being incorporated in the shell carbonate, and no marine reservoir correction data exist for Angola. Such reservoir offsets are only of the order of hundreds of years, however, in order to calibrate the two ^{14}C ages as accurately as possible we utilised the reservoir estimate of ~500 years from the NW coast of South Africa[22]. The conventional radiocarbon ages obtained, 44,650 ± 500 BP (OxA-26335) and 40,340 ± 310 BP (OxA-26336), showed good agreement with the OSL measurements. We therefore combined all OSL and ^{14}C dates together into a Phase in the program OxCal[23] (see Supplementary Data 1) to indicate that they form a coherent group but are not exact markers of the same point in time (making the assumption that the ancient shoreline survived for a finite period of time). OxCal then generated probabilities for the start, mid, and end dates of the existence of the shoreline (see Fig. 2). The median midpoint date (~45.1 ka) was used as the input in our models of uplift rate. To investigate the effects of differing depositional environment between the three sites we re-ran the model excluding the two ages from site B (near-shore, rather than lagoonal) and found negligible differences in the overall age.

We combined the ~45 ka age with different eustatic sea level curves[24;25;26;27;28] to constrain confidence intervals on uplift rates. A full discussion of the various sea-level data is given in Methods, and a visual comparison of the various curves is presented in Supplementary Figure 4. An example uplift rate calculation is given in Fig. 3a, using the curve of[24], the others are included as Supplementary Fig. 5-7. We used a terrace elevation of 23 m in the calculation, corresponding to the observed and predicted maxima in the histogram on the right hand side of panel b of Fig. 3. The maximum likelihood estimates for the uplift rates using the four sea level curves range from 2.0-2.4 mm/yr, with 90% confidence intervals defining a range of 1.8-2.6 mm/yr.

Automated correlation of terrace remnants

Independent verification of an uplift rate of ~2.2 mm/yr comes from the comparison of automatically identified terraces in the SRTMGL1 digital elevation model (DEM) with expected terrace levels from past eustatic sea-level curves (see Methods). We identify terraces in the region plotted in Fig. 1d as areas where the gradient is close to zero. Noise introduced by small, low-relief regions such as hill tops and river beds, and small-scale topography on the terrace surfaces, has the effect of breaking up even large terraces, meaning that terraces are often only poorly recovered and might not be found at all. To improve spatial coherence we thus filter the topographic gradients before calculating their magnitudes, as described in Methods. The automated extraction at Benguela agrees well with terrace heights obtained from manual identification of terraces (white dots on Fig. 3b, see Supplementary Figure 1), and has the advantage that it can resolve multiple terraces that are closely spaced in height. However, it does not recover the level at ~260 m due to its surface being heavily dissected and noticeably tilted (Fig. 1d, profile 1, also see Fig. 4).

The best-fitting uplift rates (honouring the measured age of the ~25 m terrace) for the four separate sea-level curves[24-28] are in close agreement (Fig. 3, and supplementary Figs. 5-8). In addition, these uplift rates can be used to make predictions of other terrace elevations that should be observed in the area (pale orange histograms in Fig. 3). When these are compared with the flat areas extracted from the SRTM DEM, there is a generally good agreement. In particular, the three most detailed sea-level curves[24,25,27] agree that the ~155 m terrace appears to have formed at ~80ka. Such agreement gives us additional confidence in our results, and allows us to extend the approach outside the region where we have direct constraint on terrace age.

We extended the automated terrace identification along the length of the Angolan coastline. The results are shown in Fig. 4a, with significant flood plains, alluvial terraces and water bodies removed manually, and close-up views of parts of the terrace map in Fig. 4a are given as Supplementary Figures 9-12. Fig, 4b shows the concentration of flat areas along a north-south profile, and Fig. 4c shows the same profile with noise introduced by seaward dipping fluvial systems removed (see Methods). The automated method allows lateral continuity of terraces to be traced over long distances, particularly near Luanda in the north and Namibe in the south. The terrace formed by what we model as the 81 ka high stand (at ~150 m elevation at Benguela) is particularly prominent and can be identified along virtually the entire coastline (dotted line in Fig. 4c). Doming is evident, with terraces near Luanda climbing steadily towards the south, and terraces near Namibe climbing steadily towards the north. We can construct an uplift model (Fig. 4d) and an uplift rate model (Fig. 4e) for the length of the coastline by honouring the terrace continuity, the uplift rate given by the 25 m terrace dates at Benguela, and local maxima in the correlation between observed and expected terrace elevations for different uplift rates along the coastline. These models (Fig. 4d-e) suggest a domal uplift with an amplitude of ~300 m and a diameter of >1,000 km centred near Benguela. This doming is coincident with the projection of the Bié plateau on the coastline.

Rate and origin of the Angolan uplift

The field, remote-sensing, and modelling results combine to show that the Angolan coastline has undergone rapid Pleistocene uplift relative to sea-level. A ~1.8-2.6 mm/yr uplift rate is significantly faster than the 0.12 mm/yr obtained through the analysis of long river profiles[29], which are sensitive to uplift rates on much longer time periods. The uplift is too broad to be caused by salt movements or active tectonics, especially as we see no evidence for uplift variations on the scales associated with fault segmentation (~15—20 km), and little seismicity. The southeastern Atlantic margin is 120-140 Ma old, and any rim flank uplifts due to lateral heat flow and flexure during rifting have long since subsided. The large lateral extent of the domal uplift (>1000 km) argues against a flexural control on uplift caused by sediment offshore loading following rifting, such as that proposed that the Gurupe Arch in NE Brazil[30]. The study region is also sited far from the effects of glacial loading and unloading.

We propose that the broad wavelength of uplift, the apparent association with the Bié dome, as well as the absence of viable alternatives provide compelling evidence that the uplift is caused by mantle upwelling. Tomographic images are variable in their support for a velocity anomaly beneath Angola (e.g.[31,32,33]) and yet the Bié Dome is one of the few places to retain a free-air gravity anomaly, consistent with the presence of mantle-supported dynamic topography, when an isostatic correction is applied to the African gravity field[9]. This means that the gravity high over the dome cannot be explained by isostatic compensation. A 25 mGal gravity residual is centred on the dome, which suggests that there are at least 500 m of dynamic topography[34] (Fig. 1b) assuming a long-wavelength admittance of 50 mGal/km[35].

The Pleistocene uplift event cannot have been sustained for long, as the identifiable coastal terrace sequence peaks at an elevation of ~250 m near Benguela (Fig. 1d). The 1-2 km height of the Cenomanian (93-100 Ma) surface onshore suggests a maximum total uplift in this region (e.g. [8]). At ~2 mm/yr this amount would accumulate in ~1 Ma, though both the inversion of river profiles and the deltaic deposition in the Kwanza basin suggest that uplift began at ~25 Ma. As a possible resolution to this apparent paradox, we suggest that the onset of regional uplift may have been associated with the initial impact of a mantle plume, but that the topographic expression of this plume may be modulated on shorter timescales, perhaps in processes similar to those invoked to explain the V-shaped ridges associated with the Iceland plume or inferred transient periods of uplift in the North Sea (e.g. [36,37]).

Our interpretation is that the late Pleistocene coastal uplift of Angola results from a pulse of mantle-derived uplift, providing an opportunity to study this phenomenon in an area with relatively few other complicating factors. We note that the >2 mm/yr uplift rate reported here is theoretically detectable by long-term GPS measurements, though this analysis has not yet been done to our knowledge. We are also unaware of any historical or archaeological sources that might give insight into recent uplift, though we recognize that the ~1 m of uplift expected since the Portuguese arrival would be visible in the event that any coastal historical buildings are extant, and that the hundreds of metres of uplift on this length-scale will have had an important impact on the palaeogeography of SW Africa over a time interval relevant to the study of prehistoric human populations.

Constraining the processes responsible for swells and basins within the continents has been difficult due to the lack of precise temporal and spatial limits on the uplift of topography. In Africa, for example, differing explanations are postulated for the origin of the elevated regions, ranging from whether uplift results from a large region of upwelling across southern Africa (e.g. [2; 3; 5]); as small, isolated, swells (e.g. [7; 8]); or whether the topography is not in fact supported by thermal upwelling at the present and instead results from processes such as the addition of underplated material in earlier geological periods (e.g. [6]) or rim flank uplifts to passive margin and interior rifts (e.g. [39,40]). Our results show that Pleistocene uplift of Angola occurs with a >1000 km diameter and correlates with regions of high topography, hence supporting a model of small isolated swells, at least for the Angolan uplift.

The 25 mGal residual gravity anomaly centred on the Bie Plateau suggests the presence of at least 500m of dynamic uplift. This represents the lower limit for the dynamic component and it is unclear whether there may be additional isostatic component, perhaps through the conversion of relatively short-lived pulses of ‘dynamic’ uplift into permanent isostatic uplift through the addition of crustal material during those pulses. Mantle processes have had an large effect on the recent (~1 Ma) history of the Angolan coastline and a better understanding of the crustal structure of the Bie Plateau is urgently needed to fully understand the processes that control the topography of such 'stable' margins over a variety of time scales.

Methods, including statements of data availability, code availability, and references, are available in the online version of this paper.

References

1) Vail, P.R . & Mitchum Jr, R. M. Global Cycles of Relative Changes of Sea Level from Seismic Stratigraphy: Resources, Comparative Structure, and Eustatic Changes in Sea Level. (1979)

2) Lithgow-Bertelloni, C. & Silver, P. G. Dynamic topography, plate driving forces and the African superswell. *Nature* **395,** 269-272 (1998).

3) Burke, K. & Gunnell, Y. The African erosion surface. *Geol. Soc. Am. Memoir*, **201** (2008).

4) Nyblade, A. A. & Robinson, S. W. The African Superswell. *Geophys. Res. Lett.* **21,** 765-768 (1994).

5) Gurnis, M., Mitrovica, J.X., Ritsema, J. & van Heijst, H.J. Constraining mantle density structure using geological evidence of surface uplift rates: the case of the African Superplume. G^3 **1,** 7 (2000).

6) Nyblade, A. A. & Sleep, N. H., Long lasting epeirogenic uplift from mantle plumes and the origin of the Southern African Plateau. G^3, **4,** 12 (2003).

7) Al-Hajri, Y., White, N. & Fishwick, S. Scales of transient convective support beneath Africa. *Geology* ***37*****,** 883-886 (2009).

8) Roberts, G.G. & White, N. Estimating uplift rate histories from river profiles using African examples. *J. Geophys. Res.* ***115*****,** B2 (2010).

9) Molnar, P., England, P.C., & Jones, C.H. Mantle Dynamics, isostacy, and the support of high terrain. *J. Geophys. Res.* **120,** 1932-1957 (2014).

10) Giresse, P., Hoang, C-T., & Kouyoumontzakis, G. Analysis of vertical movements deduced from a geochronological study of marine Pleistocene deposits, southern coast of Angola. *J. African Earth Sci.* **2,** 177-187 (1984).

11) Guiraud, M., Buta-Neto, A., & Quesne, D. Segmentation and differential post-rift uplift at the Angola margin as recorded by the transform-rifted Benguela and oblique-to-orthogonal-rifted Kwanza basins. *Marine Petrol. Geol.* ***27*****,** 1040-1068 (2010).

12) Karlstrom, K.E., et al. Mantle-driven dynamic uplift of the Rocky Mountains and Colorado Plateau and its surface response: Toward a unified hypothesis. *Lithosphere* ***4*****,** 3-22 (2012).

13) Crow, R., et al. Steady incision of Grand Canyon at the million year timeframe: A case for mantle-driven differential uplift. *Earth Planet. Sci. Letts.* ***397*****,** 159-173 (2014).

14) Isachsen, Y.W., Contemporary doming of the Adirondack Mountains: Further evidence from releveling. *Tectonophys.* ***71*****,** 95-96 (1981).

15) Hartley, R.A., Roberts, G.G., White, N. & Richardson, C. Transient convective uplift of an ancient buried landscape. *Nat. Geosci.* ***4*****,** 562-565 (2011).

16) Soares de Carvalho, G. Alguna problemas dos terracos quaternaries de littoral de Angola. *Bol. Serv. Geol. Min. Angola* **2,** 5-15 (1961).

17) Broecker, W.S. Preliminary evaluation of uranium series inequilibrium as a tool for absolute age measurement on marine carbonates. *J. Geophys. Res*. **68,** 2817-2834 (1963).

18) Giresse, P., Quaternary sea-level changes on the Atlantic coast of Africa. in: Sea-Level Changes, eds. Tooley, M.J., Shennan, I., Institute of British Geographers, Special Publication Series, Blackwell, Oxford. (1987).

19) Rhodes, E. J., Singarayer, J. S., Raynal, J. P., Westaway, K. E., & Sbihi-Alaoui, F. Z. New age estimates for the Palaeolithic assemblages and Pleistocene succession of Casablanca, Morocco. *Quat. Sci. Revs*. ***25*****,** 2569-2585 (2006).

20) Jacobs, Z. Luminescence chronologies for coastal and marine sediments. *Boreas*, ***37*****,** 508-535 (2008).

21) Benedetti, M.M., et al. Late Pleistocene raised beaches of coastal Estremadura, central Portugal. *Quat. Sci. Revs.* ***28*****,** 3428-3447 (2009).

22) Dewar, G., Reimer, P. J., Sealy, J. & Woodborne, S. Late-Holocene marine radiocarbon reservoir correction (Delta R) for the west coast of South Africa. *The Holocene*. **22,** 1481-1489 (2012).

23) Ramsey, C. B. Bayesian analysis of radiocarbon dates. *Radiocarbon*, ***51*****,** 337-360 (2009).

24) Waelbroeck, C., et al. Sea-level and deep water temperature changes derived from benthic foraminifera isotopic records. *Quat. Sci. Revs*. ***21*****,** 295-305 (2002).

25) Grant, K.M., et al. Sea-level variability over five glacial cycles. *Nat. Comms*. ***5*****,** (2014).

26) De Boer, B., Lourens, L.J. & Van De Wal, R.S. Persistent 400,000-year variability of Antarctic ice volume and the carbon cycle is revealed throughout the Plio-Pleistocene. *Nat. Comms.* ***5*****,** (2014).

27) Zachos, J.C., Dickens, G.R., & Zeebe. R.E., An early Cenozoic perspective on greenhouse warming and carbon-cycle dynamics. *Nature* **451,** 279-283 (2014).

28) Hansen, J., Sato, M., Russell, G., Kharecha, P. Climate sensitivity, sea level and atmospheric carbon dioxide. *Phil. Trans. Royal Soc. London A* **317,** (2013).

29) Rudge, J. F., Roberts, G. G., White, N. J., & Richardson, C. N. Uplift histories of Africa and Australia from linear inverse modeling of drainage inventories. *J. Geophys. Res.* ***120*****,** 894-914 (2015).

30) Watts, A. B., Rodger, M., Peirce, C., Greenroyd, C. J., & Hobbs, R. W. Seismic structure, gravity anomalies, and flexure of the Amazon continental margin, NE Brazil. *J. Geophys. Res.* ***114*****,** B7 (2009).

31) van der Hilst, R., Widiyantoro, S. & Engdahl, R. Evidence for deep mantle circulation from global tomography. *Nature* **386,** 578–584 (1997).

32) Begg, G.C., et al., The lithospheric architecture of Africa: Seismic tomography, mantle petrology, and tectonic evolution. *Geosphere* ***5*****,** 23-50 (2009).

33) Li, A. & Burke, K. Upper mantle structure of southern Africa from Rayleigh wave tomography. *J. Geophys. Res.* ***111*****,** B10 (2006).

34) Craig, T. J., Jackson, J. A., Priestley, K., & McKenzie, D. Earthquake distribution patterns in Africa: their relationship to variations in lithospheric and geological structure, and their rheological implications. *Geophys. J. Int.* ***185*****,** 403-434 (2011).

35) McKenzie, D. The influence of dynamically supported topography on estimates of Te. *Earth Planet. Sci. Letts*. ***295*****,** 127-138 (2010).

36) Jones, S. M., White, N., & Maclennan, J. V-shaped ridges around Iceland: Implications for spatial and temporal patterns of mantle convection. *G3* ***3*****,** 1-23 (2002).

37) Rudge, J. F., Champion, M. E. S., White, N., McKenzie, D., & Lovell, B. A plume model of transient diachronous uplift at the Earth's surface. *Earth Planet. Sci. Letts*. ***267*****,** 146-160 (2008).

38) Pedoja, K., et al., Relative sea-level fall since the last interglacial stage: are coasts uplifting worldwide?. *Earth-Science Reviews*, ***108*****,** 1-15 (2011).

39) Gilchrist, A. R., & Summerfield, M. A. Differential denudation and flexural isostasy in formation of rifted-margin upwarps. Nature **346,** 739-742 (1990).

40) Karner, G.D., et al., Distribution of crustal extension and regional basin architecture of the Albertine rift system, East Africa. *Marine Petrol. Geol.* ***17*****,** 1131-1150 (2000).

Author contributions

R.T.W. and A.B.W conceived and designed the experiments; M.T. and R.T.W. performed the fieldwork and undertook all sample collection; J-L.S. and M.T. performed the OSL sample analyses, and M.D. performed the radiocarbon calibrations and age modelling; R.L.K. constructed the method for automatic terrace extraction; B.K., R.L.K. and R.A.S. performed the regional terrace correlations; M.D., R.L.K., R.A.S., M.T., and R.T.W. co-wrote the paper.

Additional information

Supplementary information is available in the online version of the paper. Reprints and permissions information is available online at www.nature.com/reprints. Correspondence and requests for materials should be directed to RTW (richard.walker@earth.ox.ac.uk)

Acknowledgments

This project was funded by the Royal Society of London. The European Space Agency provided KOMPSAT2 imagery under project allocation C1P.6462. The use of SRTM global data was provided by the OpenTopography Facility with support from the National Science Foundation under NSF Award Numbers 1226353 & 1225810. We thank Andre Buta-Neto and Carla Tunguno (Universidad Agostinho Neto) and Paola Gomez (Benguela Museum) for help during fieldwork, the Head of the Department of Geology at Universidad Agostinho Neto for his support, and Carlos Laiginhas for organizing all fieldwork logistics.

Competing financial interests

There are no competing financial interests

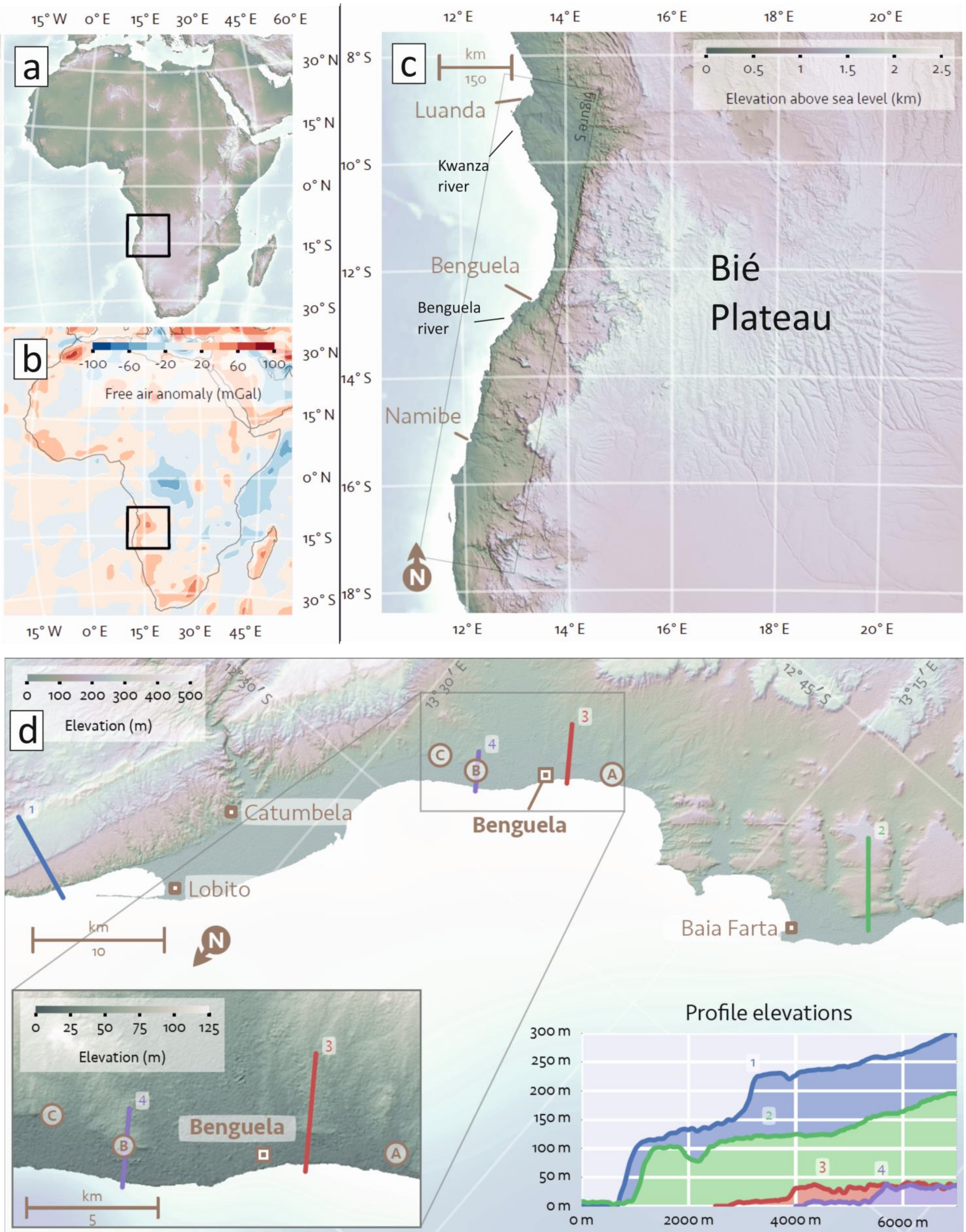

Figure 1: Regional setting of the study sites. (a,b) Topographic and Free air anomaly maps of Africa, adapted from[27]. (c) Topography of the Angolan coastline and Bie Plateau. (d) Topography of the Benguela region, with a close-up of Benguela itself as an inset. The three sample sites (A-C)

are labelled and four topographic profile lines are marked. Prominent terrace treads are visible at elevations of ~120 m, ~150 m and ~230 m adjacent to Lobito (profile 2) and Baia Farta (profile 1). Our samples are taken from the 25 m terrace (profiles 3 and 4).

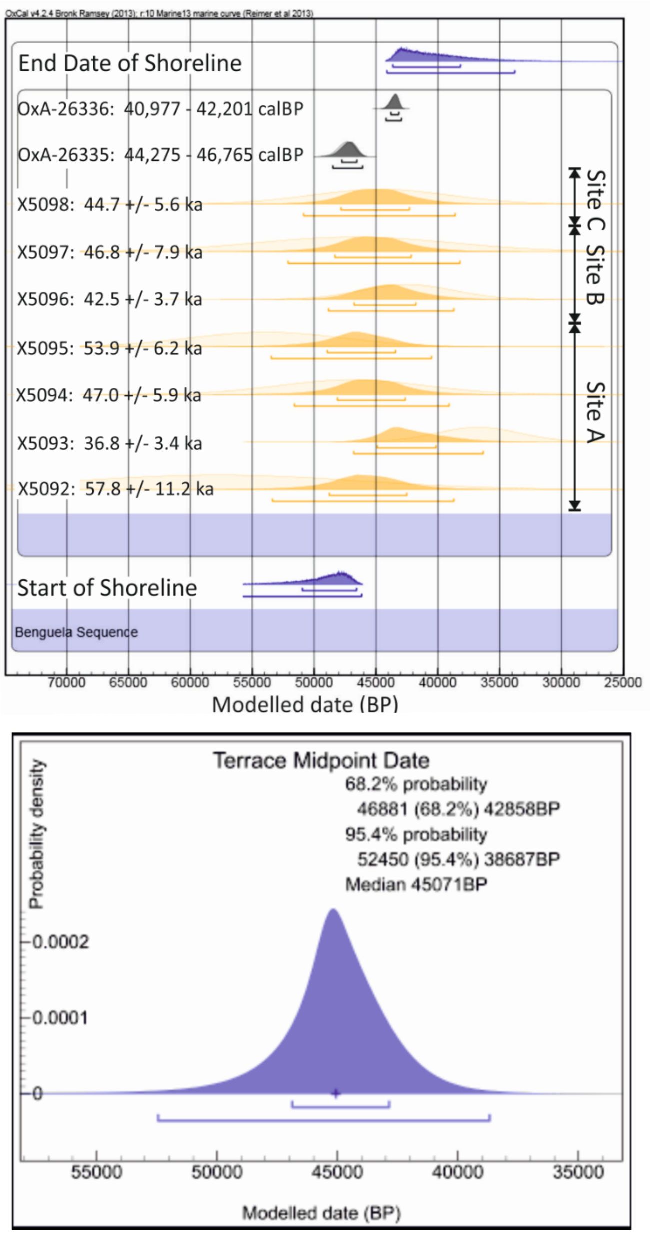

Figure 2: OxCal age model incorporating the eight OSL samples and two radiocarbon ages. Sample lab codes and ages are given in text at the left-hand side of the figure. Uncertainties are 95% for calibrated radiocarbon and 1σ for OSL. Individual sample age ranges are shown on the 'Oxcal' model plot as light colours, with the model output for each shown as the darker regions, as well as the modelled start and end date of the shoreline. The model 'mid- date' is shown in detail in the

lower panel. See methods for details of the dating methods.

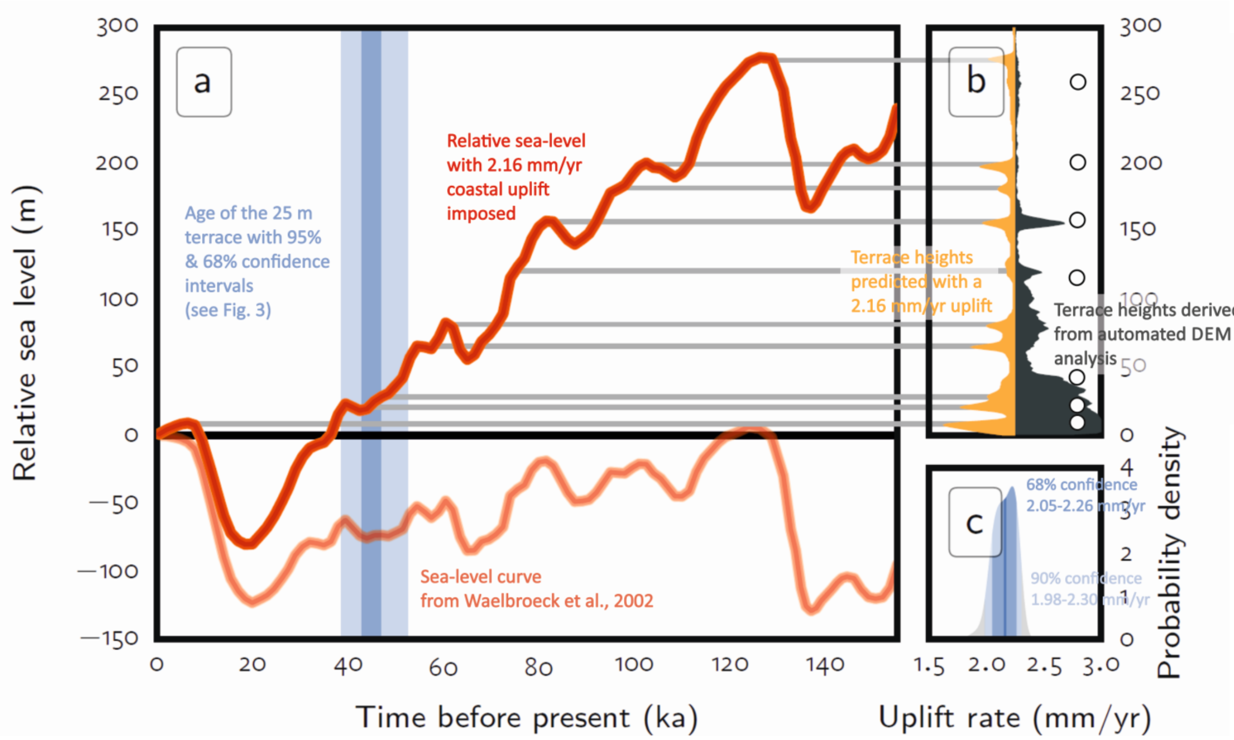

Figure 3: Uplift rates at Benguela. (a) The eustatic sea-level curve[20] is shown in pink, and the curve 'corrected' for an uplift of 2.16 mm/yr in red. The 25 m terrace age range (68% and 95%) is indicated. (b) A comparison of the distribution of automatically identified terraces near Benguela with those expected from the sea-level curve for a 2.16 mm/yr uplift. Terrace heights measured manually from the DEM are represented by white dots. (c) The terrace age probability density function is combined with the sea-level curve to give the uplift rate. This gives a maximum likelihood uplift rate of 2.16 mm/yr.

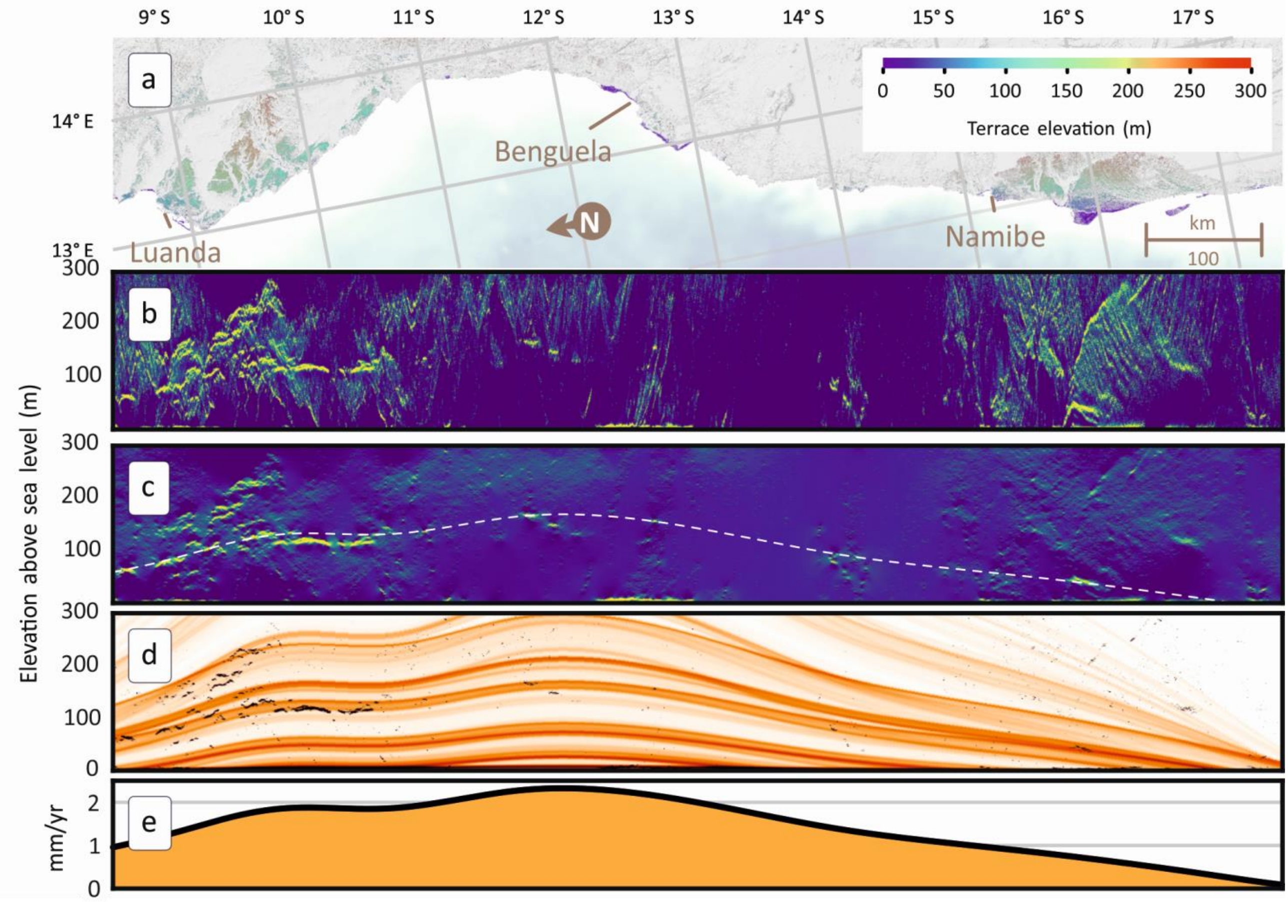

Figure 4: Regional terrace correlations. (a) Map of automatically identified terraces. (b) Normalised histograms of flat areas along the length of the map, with yellow tones indicating predominance of flat areas. (c) As before, with filtering to remove steep diagonal noise introduced by fluvial systems. The dotted line is a reconstruction of the prominent 150 m terrace at Benguela. (d) Synthetic terrace model (orange, given the uplift rates calculated from 'c') overlain on observed flat areas (black). (e) Inferred uplift rates along the coast given the interpretation of the 150 m terrace as the ~80 ka highstand.

Methods

OSL samples were collected and analysed followed standard protocols. All samples were collected in light-proof 50 x 125 mm black plastic tubes from cleaned exposures of the sections, and the ends capped. Once the sample had been extracted from the exposure, a 2" NaI probe attached to an Ortec Micronomad™ portable gamma spectrometer was inserted into the hole to measure the in-situ gamma radiation field. Samples were transported wrapped in additional light-proof bags to the Oxford University Luminescence Dating Laboratory. Additional dosimetry data was provided by ICP-MS (Inductively-Coupled Plasma Mass Spectrometry) and -AES (Atomic Emission Spectrometry) at Royal Holloway, University of London on sediment from the light-contaminated ends of the tubes discarded during sample preparation; the gamma contribution was derived from the field spectrometry, and the beta contribution was calculated from isotope concentrations derived from the mass spectrometry data.

Preparation followed conventional protocols, and began with discarding the light-contaminated ends of the tubes. Sand was pre-treated with 35% HCl and 30% H_2O_2 until the cessation of any reaction to remove, respectively, carbonates and organics. The sediment was subsequently sieved to isolate the dominant sand-sized fraction (either 125-180 µm or 180-255 µm depending on the sample), and heavy minerals were isolated with sodium polytungstate at 2.72 gcm^{-3}. 35% HF was used for 40 minutes to etch the alpha-irradiated rind of the quartz and to remove feldspars. Where subsequent testing revealed continued presence of feldspars in the samples, an additional room temperature treatment with fluorosilicic acid (H_2SiF_6) was used to ensure complete isolation of the quartz fraction. A second treatment with HCl removed precipitates and a final sieving removed any detrital fragments of grains left by the etching process.

All samples were analysed on Risø TL-DA-12 or -15 automated luminescence readers after mounting small (3-4 mm diameter) aliquots onto aluminium discs with silicone spray. All samples were analysed with a modified Single Aliquot Regeneration (SAR) protocol[41,42], incorporating a post-IR blue feldspar purity check[43]. Preheats of 260°C for the regeneration dose and 220°C for the test dose were applied on the basis of plateau tests. Dose recovery tests on a subsample of the aliquots were able to successfully recover a 120 Gy dose within ± 5%.

Between twelve and twenty-four aliquots were used for each sample, and seven regeneration points (excluding a zero-dose point, and recycling checks at both high and low doses) were typically used to characterise growth. Luminescence response of the samples was typically fairly low (400-1000 counts per 0.1s in the initial channels, with background typically around 50). Quantification of the luminescence signal was derived from the first 1 s of OSL measurement, using the subsequent 1.5 s integral of the decay curve as early background subtraction[44]. This minimizes any risk of partial bleaching resulting in age overestimation, and the consistency between 14C and OSL ages, and between OSL ages from different depositional settings (i.e. lagoonal and nearshore), also suggests that these samples are adequately bleached.

Additional quality checks included recuperation, recycling and saturation; samples which failed any of these test were excluded from further analysis. . The mean recycling ratio data for accepted aliquots was 0.98 ± 0.07, and the mean for all data 0.97 ± 0.13; both are consistent with unity. Aliquots which failed due to saturation, using $2D_0$ from a single saturating exponential fit as a criterion after[45], were used to derive minimum age estimates. Samples were best fitted with either single or double[46] saturating exponential fits, which were applied using Risø's Analyst v4.14 software, using 100 Monte Carlo repeats for error estimation. Since the use of the sum of two saturating exponentials has sometimes been reported as yielding underestimates of the true age of the order of ~10%[47,48], the recommendations of[49] are followed here, and independent chronological control has been sought from ^{14}C dating.

Single equivalent dose estimates (D_e) were derived using the Central Age Model[50], with over-dispersion values from 12-41%, and a mean of 24.4%. These values are likely to be due to the relatively low signal intensity and consequent high signal/noise ratio. Moisture content was assumed at 5±2.5 % giving a two-sigma confidence interval for time-averaged moisture content of 0-10%.

The two shell samples were radiocarbon dated at the Oxford Radiocarbon Accelerator Unit (ORAU), using routine pre-treatment and measurement protocols[51,52], and with care taken to ensure analysis of only endogenous aragonite. All of the carbonate samples prepared by ORAU are treated in parallel with the IAEA marble standard from the Cretaceous period. The particular aliquot treated at the same time as these shell samples has now been prepared 102 times by ORAU and consistently produced results that are beyond the background limit of the ^{14}C dating method.

The radiocarbon sample preparation steps are as follows. The shells were first shot-blasted with an air abrasive to remove the outer surface and expose the nacreous aragonite. The presence of calcite (which may result from recrystallization and not be endogenous to the original organism) was then tested for using Feigel's solution[53]. In both cases, the samples passed this test. The possibility that the dated fractions of the ostreida (OxA-26335) and arca (OxA-26336) shells included recrystallised aragonite is considered highly unlikely. However, in order to be as robust as possible, in addition to the Fiegels test for calcite described above, both shells were also visually inspected under a binocular microscope. The ostreida shell was very well preserved and showed no signs of either dissolution or recrystallisation; the arca shell showed limited signs of dissolution on the outer surfaces, and care was taken to avoid these areas when sampling for dating.

The shells were crushed to powder in a mortar and pestle and aliquots (~50 mg) digested overnight using concentrated H_3PO_4 in a closed rig under vacuum. The CO_2 gas liberated was trapped cryogenically, sealed into a glass ampoule and subsequently combined with a stoichiometric excess of H_2 and reduced to graphite (pure carbon) over an Fe catalyst. During this process, a small proportion of the CO_2 was diverted into a isotope-ratio mass spectrometer for $\delta^{13}C$ measurement (relative to PDB). The graphite obtained from each sample was pressed into an aluminium target and its ^{14}C activity obtained using Oxford's 2MV tandem accelerator mass spectrometer. The combined set of chronometric data was then incorporated within the same Phase of a Bayesian model in OxCal to refine the ages.

Expected terrace elevations were modelled by assuming that terraces were cut at a particular elevation whenever past sea-level was "close to" that elevation. In addition, we assume that terraces are eroded with time, with different erosion rates depending on whether or not the terrace is submerged. The likelihood $\phi(z,t)$ that at time t a terrace exists at elevation z can therefore be posed as the solution to the differential equation:

$$\frac{d\phi}{dt} = f(z - \tilde{\sigma}(t)) - \frac{\phi}{\tau}, \qquad 1$$

where f is a smoothing function that spreads the terrace cutting at any time t over a finite interval, $\tilde{\sigma}(t)$ is the relative sea-level curve adjusted for uplift history and τ is a decay parameter which differs depending on whether z is above or below sea-level at time t. The first term represents terrace cutting while the second term represents terrace erosion. f must be positive when z is near $\tilde{\sigma}(t)$ and zero elsewhere. We choose f to be a Gaussian with FWHM of 8m. The finite width represents uncertainty in the sea-level curve, as well as effects of short period variations such as tides. The model does not take into account the effects of eustatic-induced water loading and unloading on the terrace profiles. We choose τ to be given by $\tau = w_0\tau_{\mathrm{land}} + w_1\tau_{\mathrm{sea}}$, where τ_{land} and τ_{sea} represent the subærial and submarine erosion rates respectively, and $w_0 + w_1 = 1$. For consistency with f, we choose $w_0 = \int_{-\infty}^{z-\tilde{\sigma}(t)} f(z')\,dz'$ (i.e. the error function). Our results are fairly insensitive to reasonable choices of erosion rates. We choose $\tau_{\mathrm{land}} = 100$ kyr and τ_{sea} to be small enough that submerged terraces are eroded almost immediately. Finally, the relative sea-level curve $\sigma(t)$ can be adjusted for a given uplift rate history $\dot{u}(t)$ by integrating the uplift rate backwards through time, namely $\tilde{\sigma}(t) = \sigma(t) + \int_t^0 \dot{u}\,(t')dt'$. This adjustment is simply the addition of a straight line through the origin for a constant uplift rate. The terrace model can now be calculated by integrating equation 1 from the distant past until the present for elevation ranges of interest.

Automatic identification of terraces in the SRTMGL1 DEM is complicated by small low-relief regions such as hill tops and river beds, and by small-scale topography on the terrace surfaces that has the effect of breaking up even large terraces, meaning that terraces are often only poorly recovered and might not be found at all. We therefore smooth the components of the gradient vector before taking its magnitude, which is effective at augmenting the continuity of terraces. We define the smoothed gradient of the topography as $\parallel \mathcal{S}(\nabla z) \parallel = \sqrt{[\mathcal{S}(\frac{\partial z}{\partial x})]^2 + [\mathcal{S}(\frac{\partial z}{\partial y})]^2}$ where $\mathcal{S}$ is the smoothing operator and $\frac{\partial z}{\partial x}$ and $\frac{\partial z}{\partial y}$ are the N-S and E-W partial derivatives of the topography, respectively. Gaussian filters tend to shrink terraces because the slopes at the edges are blended with the slopes of adjacent areas, while median filters cause flat regions to grow by about half the window width. To mitigate these problems, we used a more sophisticated filter on the horizontal derivatives: if ξ_0 represents the data to be smoothed, in our case the partial derivatives $\frac{\partial z}{\partial x}$ or $\frac{\partial z}{\partial y}$, then the filter is defined such that the result ξ minimises the expression $\iint (\xi - \xi_0)^2 dA + s \iint \parallel \nabla \xi \parallel dA$. The coefficient s is the smoothing weight; higher values of w result in more smoothing. The advantage of this filter is that it preserves sharp edges, yet gradually removes detail with higher values of s. After calculating the smoothed gradient, we use a simple Gaussian weighting function to map the distribution of terraces, where the weighting w is given by $w = \exp(-(a \parallel \mathcal{S}(\nabla z) \parallel)^2)$. The parameter a governs how flat an area must be to be given any weighting. We used $a = 200$, meaning that only slopes of less than 0.5° are assigned any significant weight. Finally, we inspected the results visually and cut out regions that are clearly not marine cut terraces, such as flood plains, alluvial terraces and reservoirs.

Each column of the image in panel (b) in Figure 5 of the main text is a nomalised weighted histogram of the topography for a small interval along the length of the map in panel (a) from left to right. The weighting is calculated using the method above, and the histograms are normalised by subtracting a Gaussian-smoothed version of the histogram with a Gaussian window of width σ = 10 m. The histogram columns are plotted as an image coloured such that high occurrences are yellow and low occurrences are blue. Panel (c) is the same as panel (b), but the image has been filtered in the wave-number domain to cut out steep coherent signals (by removing all signals with a wave vector close to horizontal). This is analogous to *f*-*k* filtering in seismic reflection processing.

The choice of eustatic sea-level curve impacts the calculated uplift rate. In order to explore variation between different curves, we used four different eustatic sea level curves in our analyses[24-27], with d18O records in the latter converted to past sea level using equations from[28]. Before converting the d18O data from[27] to relative sea level, we used a moving Gaussian average (FWHM 4 ka) to remove data scatter. The four sea-level curves are shown superimposed for visual comparison in Supplementary Figure 4. The uplift rates at Benguela, based on our dating of the 25 m terrace, calculated from all four curves are very consistent, bounded by respective 90% confidence intervals of 2.0-2.3 mm/yr, 2.1-2.5 mm/yr, 2.2-2.6 mm/yr and 1.8-2.1 mm/yr (see Fig. 3 in the main text, and supplementary Figures 5-7). The expected uplifted terraces given different uplift rates calculated for the respective sea level curves are plotted in supplementary Figure 8.

Data availability

We used the publicly available NASA Version 3 SRTM Global 1 arc second topographic dataset. In this dataset, voids are filled using the ASTER GDEM2 for regions outside the USA. The global dataset is available for processing and download from the OpenTopography Facility (www.opentopography.org). KOMPSAT2 satellite imagery was provided under academic licence through the European Space Agency and is not for distribution. The authors declare that all other data supporting the findings of this study are available within the article and its supplementary information files.

Code availability

Enquiries about the computer code used for terrace modelling should be sent to Richard Kahle (richard.kahle@uct.ac.za).

References only in Methods

41 Murray, A.S., & Wintle, A.G. Luminescence dating of quartz using an improved single-aliquot regenerative-dose protocol. *Radiat. Meas.* **32,** 57-73 (2000).

42 Murray, A.S., & Wintle, A.G., The single aliquot regenerative dose protocol: potential for improvements in reliability. *Radiat. Meas.* **37,** 377-381 (2003).

43 Duller, G.A.T., Distinguishing quartz and feldspar in single grain luminescence measurements. *Radiat. Meas.* **37,** 161-165 (2003).

44 Ballarini, M., Wallinga, J., Wintle, A.G., & Bos, A.J.J. A modified SAR protocol for optical dating of individual grains from young quartz samples. *Radiat. Meas.* **42,** 360-369 (2007).

45 Wintle, A.G., & Murray, A.S. A review of quartz optically stimulated luminescence characteristics and their relevance in single-aliquot regeneration dating protocols. *Radiat. Meas.* **41,** 369-391 (2006).

46 Berger, G.W., & Chen, R. Error analysis and modelling of double saturating exponential dose response curves from SAR OSL dating. Ancient TL **29,** 9-14 (2011).

47 Lowick, S.E., Preusser, F., & Wintle, A.G. Investigating quartz optically stimulated luminescence dose–response curves at high doses. *Radiat. Meas.* **45,** 975-984 (2010).

48 Timar-Gabor, A., Vasiliniuc, S., Vandenberghe, D.A.G., Cosma, C., & Wintle, A.G. Investigations into the reliability of SAR-OSL equivalent doses obtained for quartz samples displaying dose response curves with more than one component. *Radiat. Meas.* **47,** 740-745 (2012).

49 Lowick, S.E., & Preusser, F. Investigating age underestimation in the high dose region of optically stimulated luminescence using fine grain quartz. *Quat. Geochronol.* **6,** 33-41 (2011).

50 Galbraith, R.F., Roberts, R.G., Laslett, G.M., Yoshida, H., & Olley, J.M. Optical dating of single and multiple grains of quartz from Jinmium rock shelter, northern Australia, part 1, Experimental design and statistical models. Archaeometry **41,** 339-364 (1999).

51 Brock, F., Higham, T. F. G, Ditchfield, P. & Bronk Ramsey, C. Current pretreatment methods for AMS radiocarbon dating at the Oxford Radiocarbon Accelerator Unit (ORAU). *Radiocarbon* **52,** 103–112 (2010).

52 Bronk Ramsey C, Higham T., & Leach P. Towards high-precision AMS: progress and limitations. *Radiocarbon* **46,** 17–24 (2004).

53 Friedman, G. M. Identification of carbonate minerals by staining methods. *J. Sediment. Petrol*. **29,** 87–97 (1959).